Hierarchical Control and Full-range Dynamic Performance Optimization of Supercapacitor Energy Storage System in Urban Railway

Feiqin Zhu, *Student Member, IEEE*, Zhongping Yang, *Member, IEEE*, Huan Xia, *Member, IEEE*, Fei Lin, *Member, IEEE*

***Abstract*—The installation of stationary supercapacitor energy storage system in urban railway system effectively improves the energy saving rate by means of recycling the train's regenerative braking energy. In this paper, a hierarchical control strategy, which consists of an energy management layer and converter control layer, is proposed. In the energy management layer, the energy management state machine is introduced. In the converter control layer, based on the double closed-loop PI control strategy, a multi-objective optimization algorithm for the outer voltage loop is proposed, which optimizes the control parameters at each operating point, comprehensively considering undershoot suppression, rapidity and anti-disturbance performance of the system. The proposed control strategy is validated through simulation and laboratory experiment, and finally applied in the MW-level energy storage device (ESD) of Beijing Batong Line.**

***Index Terms*—supercapacitor energy storage, urban rail, hierarchical control, dynamic performance, full-range optimization**

I. Introduction

With the rapid development of transportation system, the energy consumption and pollution become major concern. Therefore, energy storage systems(ESSs) are widely investigated to realize efficient electric drives in automobiles [1, 2] and rolling stocks [3, 4]. In metro system, the ESSs play the role of braking energy recovery as well as network voltage stabilization [5]. Compared with other energy storage elements such as batteries and flywheels, supercapacitors are capable of fast charging and discharging due to high power density, and have great potential of energy recovery [6]. Therefore, energy storage systems based on supercapacitors have been installed in a number of metro lines around the world [7–9].

As the voltage of supercapacitor is coupled with the state of charge (SOC) [10, 11], the utilization ratio of supercapacitor energy will be very low if the supercapacitor is directly connected to the traction supply network. Therefore, a bidirectional DC/DC converter is used as the intermediate link between the supercapacitor pack and traction network, which takes charge of the energy flow. The bidirectional buck/boost DC/DC converter, which has a small voltage stress and can be connected in series-parallel to enhance the power capability, is used most widely for energy storage systems [12–14]. Aside from this, the converter topology has also been improved in past studies, such as the three-level converter, which improves the efficiency of switching elements [15] and the cascaded converter, which flexibly selects the voltage rating at both sides of the converter [16].

The issue of ESS control refers to two aspects, i.e. power flow management between the ESSs, trains and substations [17–19], and the energy-storage converter control. For energy-storage converter control, there are mainly two variables being controlled, i.e. the supercapacitor current and the network voltage [20, 21]. The double closed-loop control strategy with proportional-integral (PI) regulators, in which the outer loop regulates voltage and the inner loop regulates current, is used widely for control of energy-storage converters, due to easy implementation of its parameter settlings [22, 23]. In order to realize high-performance control, a polynomial control method was proposed in [24], on the basis of the converter model in the discrete domain. W. Lhomme took the influence of the inductor impedance on the system stability into consideration, and proposed a maximized control structure [25]. In [26], a sliding mode control method for the bidirectional DC/DC converter was proposed. However, the inherent chattering problem of sliding mode control has yet to be solved.

On account of the high power level of the energy storage system in urban railways [27], the linear control method based on PI regulators is still the mainstream in practical application for the purpose of ensuring reliability of the system. The distinctiveness for the converter in the application field of urban rail systems is that the system operates intermittently, which requires rapid response to the shock of the vehicle's regenerative braking current [28]. In addition, there is wide-range variation of the train current, supercapacitor voltage and network voltage, influencing the steady and dynamic performance of the DC/DC converter, which is ignored by the above papers. Therefore, designing the control strategy for the DC/DC converter at different operating points will be

Manuscript received March 31, 2017; revised August 31, 2017; accepted September 29, 2017. This work was supported in part by the National Key Research and Development Program of China under Grant 2017YFB1201105-05 (2017-2020) and the Fundamental Research Funds for the Central Universities of China under Grant 2017YJS182.

Feiqin Zhu, Zhongping Yang and Fei Lin are with the School of electrical engineering, University of Beijing Jiaotong, Beijing, 100044, China. (e-mail: 15117405@bjtu.edu.cn; zhpyang@bjtu.edu.cn; flin@bjtu.edu.cn).

Huan Xia is with the Beijing Institute of Space Launch Technology, Beijing, 100076, China. (e-mail: huanhuan7000@gmail.com).

This article has been accepted for publication in a future issue of this journal, but has not been fully edited. Content may change prior to final publication. Citation information: DOI 10.1109/TIE.2017.2772174, IEEE Transactions on Industrial Electronics

one aspect of research in the present paper.

This paper is organized as follows: First, the working principle and hierarchical control strategy of the stationary supercapacitor energy storage system is presented. Then the holistic small-signal model is established, based on which the influence of steady-state variation on the system dynamic performance is analyzed. Next, a full-range optimization algorithm for the outer loop control parameters is proposed to acquire the optimal performance at each operating point. Finally, the system model and control strategy are verified via simulation, laboratory experiment and field test.

II. ESD IN URBAN RAIL AND ITS CONTROL

A. stationary supercapacitor energy storage system

As the unidirectional diode rectifier cannot feed the DC power of the urban rail system back to the AC grid, the stationary supercapacitor energy storage system (SCESS) is installed to recycle the regenerative energy of the braking train. The traction power supply system of the urban railway with SCESSs is shown in Fig. 1, where $u_{\rm ss}$ and $i_{\rm ss}$ respectively denote the voltage and current of the rectifier, $u_{\rm esd}$ is the high-side voltage of the energy storage device (ESD), and $u_{\rm sc}$ is the supercapacitor voltage. The traction substations convert the AC medium-voltage power source (10 or 35 kV) to the urban rail power of DC 750 V (or 1500 V), and provide traction energy for trains. In this paper, the ESD is supposed to be installed in the traction substation, in parallel with the rectifier, and the supercapacitor is connected to the traction network with a bidirectional DC/DC converter.

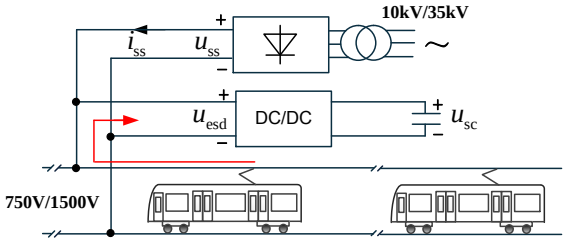

Fig. 1. Diagram of the traction power system with SCESS.

B. hierarchical control of SCESS

In order to logically control ESDs in urban rail systems, this paper proposes a hierarchical control structure, as depicted in Fig. 2. The control strategy is separated into two layers, i.e. the energy management layer and converter control layer, and latter is embedded in the former layer. The energy management layer determines the operating states of supercapacitor according to $u_{\rm sc}$, $i_{\rm ss}$ and $u_{\rm esd}$, sends corresponding voltage instruction, which is $u_{\rm ch}$ in charge state, and $u_{\rm ds}$ in discharge state to the converter control layer. The converter control layer directly controls the supercapacitor current and stabilizes the network voltage at $u_{\rm ch}$ or $u_{\rm ds}$.

In this paper, the energy management layer operates as a state machine, as seen in Fig. 3. Five states are defined, including the standby state, the charging state, the discharging state, the high-charge hold state and the low-charge hold state.

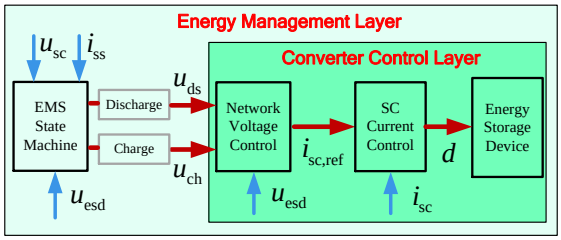

Fig. 2. Structure of the hierarchical control strategy.

It executes a state transition when the transition condition in the current state is satisfied. When the network voltage $u_{\rm esd}$ is higher than the charge threshold $u_{\rm ch,th}$, the system operates in charge state, the state machine will send the voltage reference $u_{\rm ch}$ ($\geq u_{\rm ch,th}$) to the converter control layer. When the rectifier current $i_{\rm ss}$ is larger than zero, which means the network voltage is pulled down by the traction trains, the system transfers to the discharge state. In high-charge hold or low-charge hold state, charge and discharge behavior are forbidden. For the low-charge hold state, only when the condition $u_{\rm esd} > u_{\rm ch}$ is satisfied will the ESD returns the charge state, and for the high-charge hold state, the ESD transfers to the discharge state when $i_{\rm ss} > 0$. The advantage of the state machine is that it switches the system to the expected state steadily, sends relevant instructions to the converter control layer, thus satisfying the power requirement of the traction network, protecting supercapacitor from full charge/discharge, and preventing state oscillation. Besides, the discharge behavior is triggered by the substation current, which weakens the influence of no-load voltage fluctuation.

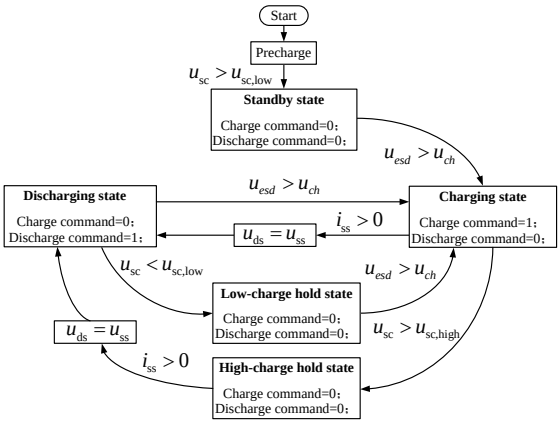

Fig. 3. The state machine for energy management layer.

In the converter control layer, the voltage-current double closed loop control structure is adopted, as seen in Fig. 4. The voltage reference $u_{\rm esd,ref}$ is obtained from the energy management layer, which equals $u_{\rm ch}$ in charge state, and equals $u_{\rm ds}$ in discharge state, as seen in (1). $G_{\rm vc}$ and $G_{\rm ic}$ represent the voltage regulator of the outer loop and current regulator of the inner loop, respectively. $u_{\rm s,up}$ and $u_{\rm s,down}$ are the upper and lower limits of the reference current. The outer loop regulates the network voltage $u_{\rm esd}$, generating reference current $i_{\rm L,ref}$ for the inner loop, and the inner loop controls

the supercapacitor current by adjusting duty cycle of the IGBT driving pulse. Under the condition of train braking, u_{esd} rises, negative voltage error is obtained by subtracting $u_{\mathrm{esd,ref}}$ from u_{esd}. Thereafter, the voltage regulator generates negative current reference $i_{\mathrm{L,ref}}$, and the current controller regulates the supercapacitor current to the reference value. Therefore, the surplus braking energy is charged to the supercapacitor, and the network voltage ceases rising. Analogously, during train traction, the voltage regulator generates positive current instruction, and the supercapacitor releases energy to stabilize the network voltage at u_{ds}.

$$u_{\mathrm{esd,ref}} = \begin{cases} u_{\mathrm{ch}}, \text{Charge command = 1} \\ u_{\mathrm{ds}}, \text{Discharge command = 1} \end{cases} \tag{1}$$

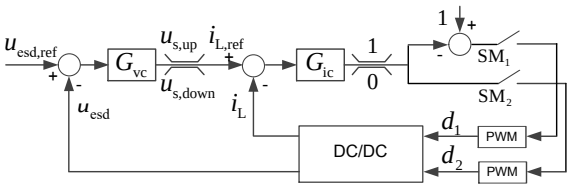

Fig. 4. The converter control layer(double-closed loop control).

From the perspective of control objective, the goal of the energy management layer is to optimize the power flow of the traction power network by adjusting the charge/discharge voltage references, thus improving the energy efficiency of the power supply system. And the goal of the converter control layer is to track the voltage instructions of the energy management layer rapidly and stably. The dynamic performance of the converter control layer is essential to the voltage stabilization and braking energy recovery effect, which is the focus of the following paper.

III. Dynamic Performance Optimization for Converter in SCESS

A. Holistic model of SCESS

In this paper, a holistic model, which includes the supercapacitor, DC/DC converter, the substation and equivalent load of trains, is established. The train is modeled as a current source i_{t}, which satisfies $i_{\mathrm{t}} = p_{\mathrm{t}}/u_{\mathrm{t}}$. So the equivalent load to one branch of the ESD is $i_{\mathrm{r}} = i_{\mathrm{t}}/N_{\mathrm{bch}}$. The substation is modeled as a branch that consists of a diode, an equivalent resistance and a voltage source. And the supercapacitor is modeled as a voltage source in series with the equivalent internal resistance, as the change of the supercapacitor voltage is very slow, influencing the steady state of the DC/DC converter instead of the dynamic behavior.

The topology of the holistic energy storage system is depicted in Fig. 5. u_{ss0} and R_{ss} are the no-load voltage and equivalent resistance of the substation. C_{f} and R_1 are the capacitance and equivalent resistance of the filter capacitor, and L and R_2 are the inductance and equivalent resistance of the filter inductor. The supercapacitor is connected with the DC/DC converter at the low-voltage side, where R_3 is

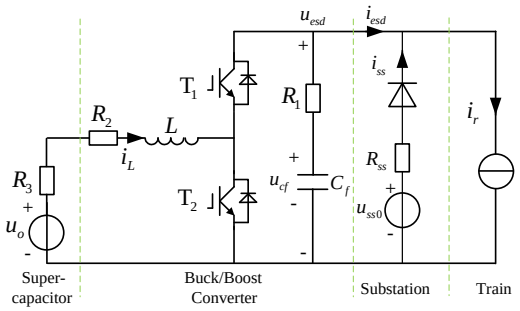

Fig. 5. Circuit structure of energy storage device.

the equivalent internal resistance of the supercapacitor and u_o represents the voltage of its capacitive part.

The energy storage system is modeled with the state-space averaging method. In this paper, the converter models under charge and discharge conditions are unified, as the converter is regarded as a boost converter with current direction reversed in charge condition. For convenience, $R_2 + R_3$ is denoted by R_{23}, and the duty cycle of the driving pulse is denoted by d. The averaged state equation is formulated as (2).

$$\begin{aligned} \begin{bmatrix} \frac{\mathrm{d}i_{\mathrm{L}}}{\mathrm{d}t} \\ \frac{\mathrm{d}u_{\mathrm{cf}}}{\mathrm{d}t} \end{bmatrix} &= \begin{bmatrix} -\frac{R_{23}+(1-d)R_1}{L} & -\frac{1-d}{L} \\ \frac{1-d}{C_{\mathrm{f}}} & 0 \end{bmatrix} \begin{bmatrix} i_{\mathrm{L}} \\ u_{\mathrm{cf}} \end{bmatrix} \\ &+ \begin{bmatrix} \frac{R_1(1-d)}{L} & \frac{1}{L} \\ -\frac{1}{C_{\mathrm{f}}} & 0 \end{bmatrix} \begin{bmatrix} i_{\mathrm{esd}} \\ u_{\mathrm{o}} \end{bmatrix} \end{aligned} \tag{2}$$

$$[u_{\mathrm{esd}}] = \begin{bmatrix} (1-d)\,R_1 & 1 \end{bmatrix} \begin{bmatrix} i_{\mathrm{L}} \\ u_{\mathrm{cf}} \end{bmatrix} + \begin{bmatrix} -R_1 & 0 \end{bmatrix} \begin{bmatrix} i_{\mathrm{esd}} \\ u_{\mathrm{o}} \end{bmatrix} \tag{3}$$

In the steady state, the state variables satisfy $\mathrm{d}i_{\mathrm{L}}/\mathrm{d}t = 0$, $\mathrm{d}u_{\mathrm{cf}}/\mathrm{d}t = 0$, and the steady-state solution is obtained from (2) and (3):

$$\begin{bmatrix} I_{\mathrm{L}} \\ U_{\mathrm{cf}} \end{bmatrix} = \begin{bmatrix} \frac{1}{1-D} & 0 \\ \frac{-R_1D(1-D)-R_{23}}{(1-D)^2} & \frac{1}{1-D} \end{bmatrix} \begin{bmatrix} I_{\mathrm{esd}} \\ U_{\mathrm{o}} \end{bmatrix} \tag{4}$$

$$[U_{\mathrm{esd}}] = \begin{bmatrix} \frac{-R_1D(1-D)-R_{23}}{D^2} & \frac{1}{1-D} \end{bmatrix} \begin{bmatrix} I_{\mathrm{esd}} \\ U_{\mathrm{o}} \end{bmatrix} \tag{5}$$

Exerting disturbance on (4) and (5), and ignoring the quadratic terms yields the linearized dynamic equation. Then we apply the Laplace transformation, and solve the state variables and output variable, which are expressed as follows:

$$\begin{aligned} \hat{i}_{\mathrm{L}}(s) = &\frac{1}{Ls + R_{23} + (1-D)\,R_1} \cdot \\ &\begin{pmatrix} -(1-D)\,\hat{u}_{\mathrm{cf}} + R_1(1-D)\,\hat{i}_{\mathrm{esd}} \\ +\hat{u}_o + (U_{\mathrm{cf}} + R_1 I_{\mathrm{L}} - R_1 I_{\mathrm{esd}})\,\hat{d} \end{pmatrix} \end{aligned} \tag{6}$$

$$\hat{u}_{\mathrm{cf}}(s) = \frac{(1-D)\,\hat{i}_{\mathrm{L}}(s) - I_{\mathrm{L}}\hat{d}(s) - \hat{i}_{\mathrm{esd}}(s)}{Cs} \tag{7}$$

$$\hat{u}_{\mathrm{esd}}(s) = (1 + R_1 Cs)\,\hat{u}_{\mathrm{cf}}(s) \tag{8}$$

Generally, the supercapacitor discharges when the network voltage u_{esd} is lower than the no-load voltage of substation,

and charges vice versa. So in charge condition, the diode of the substation branch cuts off. The ESD output current i_{esd} is expressed by (9).

$$i_{\mathrm{esd}} = \begin{cases} i_{\mathrm{r}}, \text{charging} \\ i_{\mathrm{r}} - \left(u_{\mathrm{ss0}} - u_{\mathrm{esd}}\right)/R_{ss}, \text{discharging} \end{cases} \tag{9}$$

The system equivalent block diagram is deduced from (6), (7), (8) and (9), as shown in Fig. 6. The transfer function from the supercapacitor current to the network voltage G_{vi} is obtained, which is given by (10) and (11). Considering that the inner current loop is much faster than the outer voltage loop, the influence of $\hat{u}_{\mathrm{cf}}$ and $\hat{u}_{\mathrm{esd}}$ on the inner loop is neglected in discharge condition.

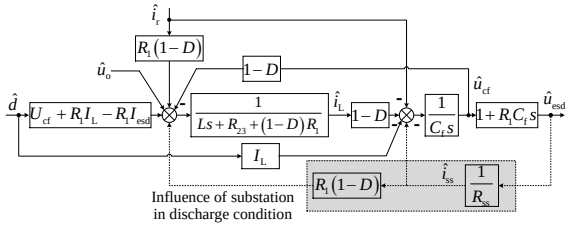

Fig. 6. The equivalent block diagram of the energy storage system.

$$G_{\mathrm{vi}}(s)|_{\mathrm{charging}} = \frac{\left(CR_1s+1\right)}{\left(U_{\mathrm{cf}}-R_1+I_{\mathrm{L}}R_1\right)C_{\mathrm{f}}s+I_{\mathrm{esd}}} \cdot \frac{}{\left[-I_{\mathrm{L}}Ls+(1-D)U_{\mathrm{cf}}-I_{\mathrm{L}}R_{23}-(1-D)R_1\right]} \tag{10}$$

$$G_{\mathrm{vi}}|_{\mathrm{discharging}} \approx \frac{R_{\mathrm{ss}}\left(R_1C_{\mathrm{f}}s+1\right)}{\left[\left(R_{\mathrm{ss}}+R_1\right)C_{\mathrm{f}}s+1\right]\cdot\left(U_{\mathrm{cf}}+DR_1I_{\mathrm{L}}\right)} \cdot \frac{}{\left[-I_{\mathrm{L}}Ls+(1-D)U_{\mathrm{cf}}-I_{\mathrm{L}}R_{23}-(1-D)I_{\mathrm{esd}}R_1\right]} \tag{11}$$

B. Influence of steady-state on dynamic performance

It can be seen from (10) and (11) that $G_{\mathrm{vi}}(s)$ has two open-loop zeros and one open-loop pole, as shown in (12). The zero z_1 arises from the equivalent resistor of the filter capacitor, which has an effect in high frequency, thus can be neglected. The zero z_2 is relevant the inductor current I_{L} and supercapacitor voltage U_{o}.The pole p is constant in discharge condition, but influenced by the ESD output current I_{esd} and the filter capacitor voltage U_{cf} in charge condition.

$$\begin{aligned} z_1 &= -1/\left(R_1C_{\mathrm{f}}\right), z_2 = U_{\mathrm{o}}/\left(I_{\mathrm{L}}L\right), \\ p &\approx \begin{cases} -I_{\mathrm{esd}}/\left(U_{\mathrm{cf}}C_{\mathrm{f}}\right), \text{charging} \\ -1/\left(R_{ss}+R_1\right)C_{\mathrm{f}}, \text{discharging} \end{cases} \end{aligned} \tag{12}$$

Taking the MW-level ESD (see Section. V-B) as an example, the influence of steady-state variation on system performance is analyzed. The ESD has eight branches in parallel, and the parameters of one branch are used for simulation, which are listed in Table. I. As there is coupling relationship between steady-variables I_{esd}, I_{L}, and U_{o}, U_{esd} and D (see (4) and (5)), the following discussion mainly concerns the variation of I_{esd} and D.

The bode diagram of G_{vi} and the distribution graphs of zero z_2 and pole p under different I_{esd} in discharge condition are plotted, as seen in Fig. 7 (a)-(c). It's seen that in discharge condition, zero z_2 locates in the right half plane and the pole p is in the left half plane, which means that the system is non-minimum phase. Besides, when I_{esd} increases from 30A to 150A, the value of z_2 reduces from 7390 to 1460. As the zero affects the corner frequencies of the system, the log-magnitude curve and the phase-angle curve also move obviously. In particular, the phase-angle lags more in medium frequency range with the increase of I_{esd} and decrease of the positive zero. In charge condition, the influence of I_{esd} on the system characters is shown in Fig. 8 (a)-(c). In contrast with that in discharge condition, the zero z_2 becomes negative but the pole p is positive, which means the system is open-loop unstable. As a matter of fact, p is canceled by a positive zero of G_{id}, and the system has a hidden instability. The system frequency response is also influenced by I_{esd} significantly.

TABLE I
PARAMETERS OF THE MW-LEVEL ENERGY STORAGE SYSTEM.

Parameters	Symbols	Vaules	Unit
filter capacitance	C_{f}	12	mF
inductance	L	1.5	mH
resistance	R_1	1	mΩ
resistance	R_{23}	18.5	mΩ
switching frequency	f_{sw}	3000	Hz

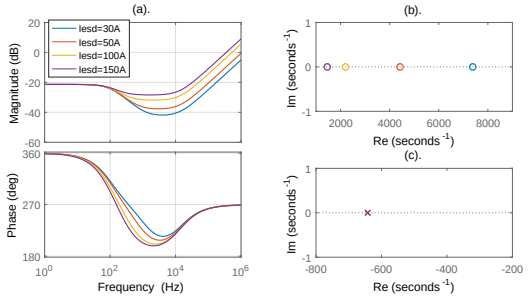

Fig. 7. Influence of I_{esd} on G_{vi} in discharging condition.

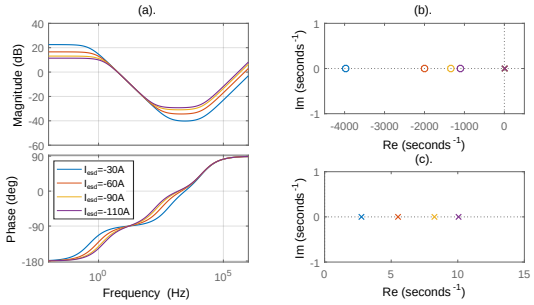

Fig. 8. Influence of I_{esd} on G_{vi} in charging condition.

The influence of D on the system characters is shown in Fig. 9 and Fig. 10. It's observed that when D increases, the zero z_2 is moving closer to the origin while p remains unchanged. Therefore, the phase-angle in the middle frequency range lags more in discharge condition and is getting more ahead in charge condition with the increase of D.

This article has been accepted for publication in a future issue of this journal, but has not been fully edited. Content may change prior to final publication. Citation information: DOI 10.1109/TIE.2017.2772174, IEEE Transactions on Industrial Electronics

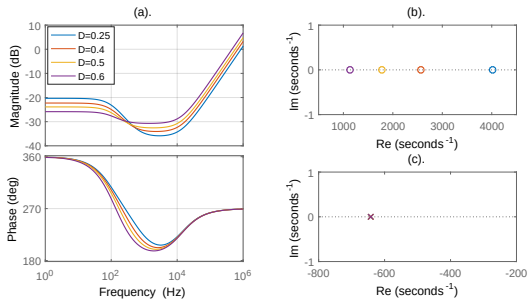

Fig. 9. Influence of D on G_{vi} in discharging condition.

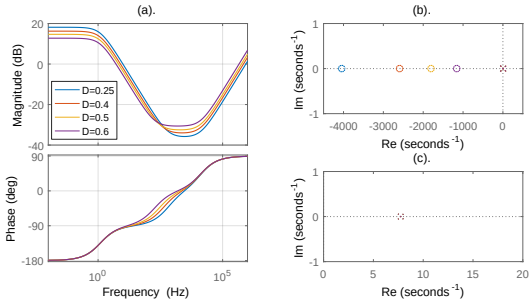

Fig. 10. Influence of D on G_{vi} in charging condition.

According to the above analysis, the frequency response and zero-pole distribution of G_{vi} is significantly affected by the ESD output current and duty cycle, which will change in a wide range during system operation. In addition, G_{vi} has a right half plane zero (RHPZ) under the discharge condition, and a positive pole under the charge condition. It is known that systems with positive zeros exhibit undershoot in the step response, which deteriorates the dynamic performance of the system and may lead to instability. Therefore, in the design of the outer loop controller, the non-minimum phase characteristic and wide variation of operating point must be taken into full consideration.

C. optimization of outer loop control parameters

For the purpose of eliminating the influence of steady-state variation on the system dynamic performance, a full-range optimized voltage loop control strategy is proposed, as depicted in Fig. 11. The parameters of the voltage loop regulator G_{vc} are optimized at each operating point (D, I_{esd}), which are represented by $K_{\mathrm{p.opt}}$ and $K_{\mathrm{i.opt}}$. During system operation, $K_{\mathrm{p.opt}}$ and $K_{\mathrm{i.opt}}$ are updated in real time according to current values of I_{esd} and D. As the system invokes optimal control parameters at each operating point, it achieves good dynamic performance in full operating range.

Apart from steady-state variation, the effect of the RHPZ should also be taken into account in the design of voltage loop regulator. Moreover, the train current changes abruptly during train accelerating and braking, which can be regarded as a frequent disturbance to the energy storage system. Therefore, the anti-disturbance performance of the voltage regulator has a significant influence on the voltage stabilization effect. In this paper, the multi-objective optimization function is formulated,

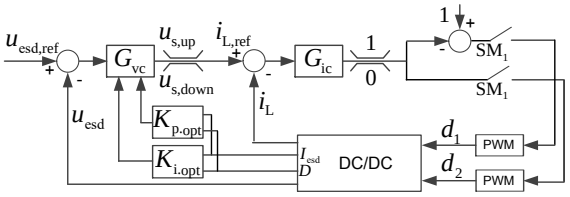

Fig. 11. Schematic diagram of full-range optimized double closed-loop control strategy.

comprehensively considering the undershoot suppression, rapidity and anti-disturbance performance of the system.

Fig. 12 (a) shows the step response of network voltage. Due to the effect of the RHPZ, u_{esd} does not increase immediately. Instead, it decreases during $[t_1, t_2]$, which exhibits the phenomenon of undershoot. The undershoot suppression index J_{ng} is formulated as (13), which will increase with the growth of $e_{\mathrm{ng}}(t)$ and prolonging of time interval $t_2 - t_1$, so the undershoot can be effectively reduced by minimizing J_{ng}.

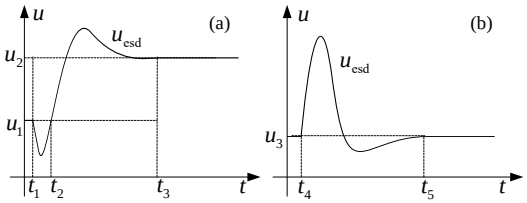

Fig. 12. Voltage response curve of u_{esd}.

$$J_{\mathrm{ng}} = \int_{\mathrm{t_1}}^{t_2} e^{e_{\mathrm{ng}}(t)} dt \tag{13}$$

$$e_{\mathrm{ng}}(t) = u_1 - u_{\mathrm{esd}}(t) \tag{14}$$

As the charge/discharge power of supercapacitor is managed by adjusting the charging/discharging voltage command (see Section. II-B), it is required that the system tracks the charging/discharging voltage command steadily and rapidly. Therefore, the rapidity index J_{ts} is proposed, as seen in (15).

$$J_{\mathrm{ts}} = \int_{\mathrm{t_2}}^{t_3} |u_{\mathrm{esd}} - u_2|^2 e^t dt \tag{15}$$

The sum of J_{ng} and J_{ts} is used to evaluate the dynamic tracing performance of the system, as shown in (16).

$$J_1 = J_{\mathrm{ng}} + J_{\mathrm{ts}} \tag{16}$$

The abrupt change of train current will cause network voltage deviation from the reference value, as illustrated in Fig. 12 (b). Therefore, the anti-disturbance performance index J_2 is proposed to reduce voltage fluctuation under the train current disturbance, as seen in (17).

$$J_2 = \int_0^T |u_{\mathrm{esd}} - u_3|^2 e^t dt \tag{17}$$

This article has been accepted for publication in a future issue of this journal, but has not been fully edited. Content may change prior to final publication. Citation information: DOI 10.1109/TIE.2017.2772174, IEEE Transactions on Industrial Electronics

The overall optimization objective J is the weighted sum of sub-objective J_1 and J_2.

$$J = \omega J_1 + (1-\omega) J_2 \tag{18}$$

Where ω is the weighting factor of the objective function J_1. Properly allocating the weights of J_1 and J_2 achieves favorable trade-off between the dynamic performance and anti-disturbance ability of the system. The cutoff frequency ω_{cv} of the voltage loop is restricted within 1/10 of the cutoff frequency of the current loop to prevent the influence of the current loop on the voltage loop.

The flow chart of the full-range parameter optimization algorithm is shown in Fig. 13. The control parameters K_{p} and K_{i} are optimized at each operating point (D, I_{esd}) with the genetic algorithm. Each individual represents a design point (K_p, K_i). The performance index J is calculated by substituting (D, I_{esd}) and (K_p, K_i) into the transfer functions, and solving the responses to the step reference and disturbance. The genetic algorithm executes the genetic operators and generates the next population with improved fitness. The algorithm terminates when the control parameters of all steady-state points are optimized. Finally, in order to implement real-time calculation of the optimal control parameters when the operating condition of the ESD changes, the optimization results are fitted with the least square method, and written into the DSP program as a function of D and I_{esd}.

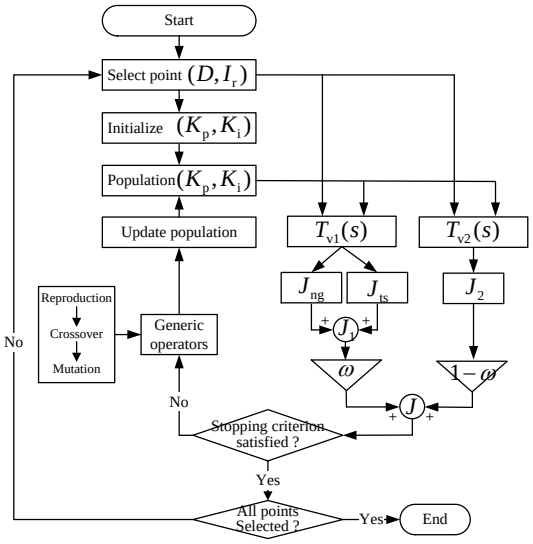

Fig. 13. Optimization algorithm for control parameters of outer voltage regulating loop.

IV. Case Study and Simulation Analysis

A. Optimization results

With the optimization algorithm proposed in last section, the control parameters K_p and K_p of the voltage outer loop are optimized when the weighting factor ω is 1, 0.5 and 0.1. The system parameters are listed in Table I . The optimization results under different ω are compared in Fig. 14. Fig. 14 (a) and (b) shows the responses of u_{esd} to step voltage reference and step disturbance of train current in discharge condition. The undershoot phenomenon becomes more serious when ω is small. And in the charge condition, the influence of ω on the voltage responses is shown in Fig. 14 (c), (d). With the increase of ω, the response to step disturbance of train current deteriorates: the voltage deviation increases and the recovery time is longer. Particularly when ω=1, the recovery time is 5 times longer than that when ω=0.1. Therefore, the weighting factor ω should be selected reasonably according to the system state and control target. The system reaches good compromise between the dynamic performance and anti-disturbance ability under the charge and discharge conditions when the control parameters are optimized under ω=0.5. The optimization results under ω=0.5 are shown in Fig. 15 .

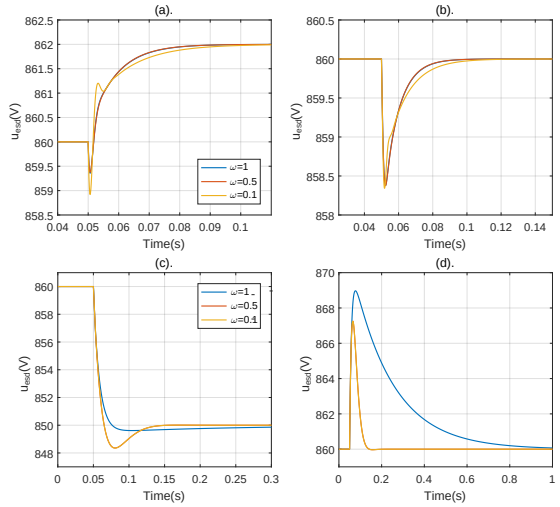

Fig. 14. Influence of ω on the voltage loop performance in discharging/charging conditions.

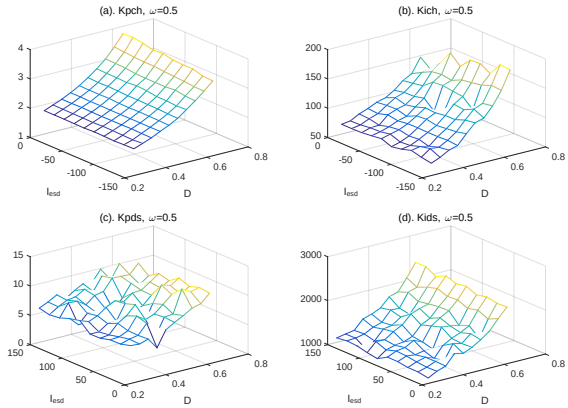

Fig. 15. The optimization results of voltage controller parameters.

B. Simulation result

Based on the optimization results under ω=0.5, the performance of the controller G_{vc} is analyzed. Fig. 16 (a) and (b) are step responses to the voltage reference at different operating point in discharge condition. The reference of u_{esd} rises from 860V to 862V at 0.5s. It's observed that the undershoot is

This article has been accepted for publication in a future issue of this journal, but has not been fully edited. Content may change prior to final publication. Citation information: DOI 10.1109/TIE.2017.2772174, IEEE Transactions on Industrial Electronics

effectively suppressed, which is less than 2V, and the transient process is very rapid, which is within 50ms when D varies from 0.25 to 0.6 and $I_{\rm esd}$ varies from 8A to 150A. Figs. 16 (c) and (d) show the responses curves to step disturbance of train current at different operating points. $i_{\rm r}$ steps at 0.5s with a step amplitude of 15A. The maximum voltage drop of $u_{\rm esd}$ is 2V, which occurs when D=0.6. The voltage fluctuation is rather small in discharge condition, as the substation also supplies power during abrupt change of train current. And the recovery time is within 50ms in the full variation range of D and $I_{\rm esd}$.

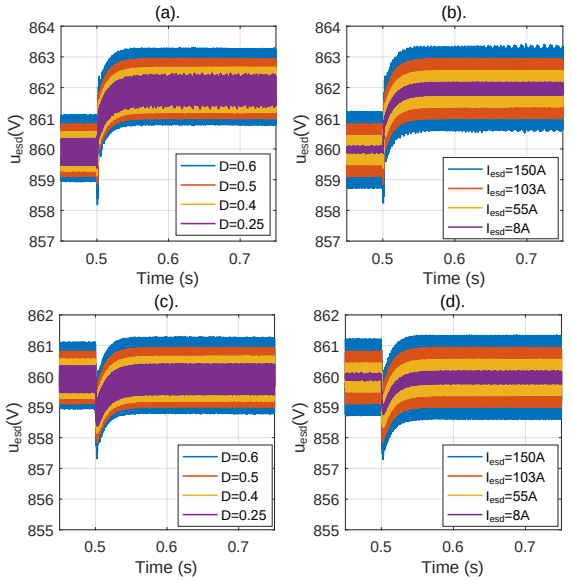

Fig. 16. Step response of the corrected outerloop in discharging Condition.

The step responses of $u_{\rm esd}$ in charge condition are shown in Figs. 17 (a), (b). The voltage reference reduces from 860V to 850V at 0.5s. As $G_{\rm vi}$ has no positive zero in charge condition, the step responses don't exhibit undershoot. Besides, the response curves at different operating points have good consistency, and the settling time is within 100ms. Figs. 17 (c) and (d) are responses of $u_{\rm esd}$ to step disturbance of train current $i_{\rm r}$. $i_{\rm r}$ steps at 0.5s with an amplitude of 15A. It's observed that the maximum voltage fluctuation is 7.3V and the recovery time is within 150ms. The system has good performance of anti-disturbance.

Therefore, in comparison with the traditional control strategy, the multi-objective optimization strategy proposed in this paper adjusts the control parameters according to the system operating point in real-time, preventing performance deterioration when the duty cycle D and ESD current $I_{\rm esd}$ vary, and achieving satisfactory performance in the full operating range. And the three optimization objectives, including the rapidity index, the undershoot suppression index and the anti-disturbance index are optimized simultaneously, so the energy storage system tracks the voltage reference stably and rapidly, weakening the influence of train current disturbance and the RHPZ in discharging condition.

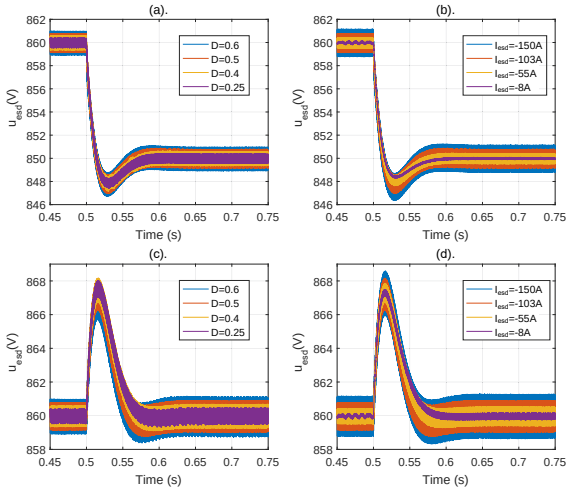

Fig. 17. Step response of the corrected outerloop in charging Condition.

V. Experimental Verification

A. Laboratory experiment

A 200 kW supercapacitor energy storage device and an experimental platform which emulates the operation of urban rail systems are developed in the laboratory, as shown in Figs. 18. The parameters of the prototype are listed in Table. II. The supercapacitor pack is connected with four Maxwell 125 V / 63 F modules in series and two in parallel, with a total storage energy of 1.09 kWh. In the emulation platform, the transformer and rectifier convert the AC 380 V power source to DC 750 V, emulating the power supply system in urban railway, and the motors with traction converters emulate the train operation.

TABLE II
Parameters of the 200kW Prototype.

Parameters	Values	Unit
filter capacitance	5	mF
chopper inductance	2.5	mH
network voltage	700-1000	V
output volage	100-500	V
output current	400	A
total capacitance of supercapacitor	31.5	F

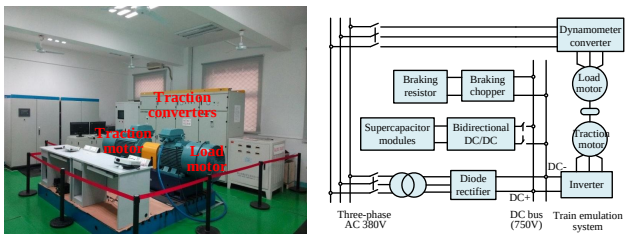

(a) (b)

Fig. 18. Diagram of the experimental platform.

Firstly, the dynamic performance of the proposed optimization algorithm for voltage outer loop is tested under differnet

conditions. Based on the parameters of the 200kW ESD, the control parameters are optimized using the optimization algorithm in Section. III-C. The optimization results are fitted and written into the DSP program. Fig. 19 (a) shows the network voltage responses in charge condition when the reference voltage steps from 950 V to 850 V. Four different operating points are tested, corresponding to the supercapacitor voltage of 285V, 405V, 235V, 405V, and the motor works in braking mode with two power values of 30kW and 15kW. In the test process, the supercapacitor charging current increases at first to absorb the DC bus energy, and the DC bus voltage quickly decreases to follow the change of reference value. Finally the supercapacitor current returns to its initial value, and the bus voltage is stabilized at the reference value. The adjusting process is within 120ms, and the voltage overshoot is within 20%. Since the inductor current reaches the limit value during the voltage loop regulation, the actual settling time is a bit longer than that in the theoretical analysis and simulation. The response curves at the four tested points have good consistency, indicating that the rapidity of the system is guaranteed at different operating points. The voltage responses to step disturbance of train current are depicted in Figs. 19 (b). The motor braking power steps from 15 kW to 30 kW when the supercapacitor voltage is 274 V and 383V, respectively. It's necessary to note that limited by ability of the motor platform, the change of motor power cannot be instantaneous, instead it rises within a slope. During this process, the supercapacitor current quickly rises with the abrupt increase of braking power, and the bus voltage is almost unchanged, the system exhibits good anti-disturbance performance.

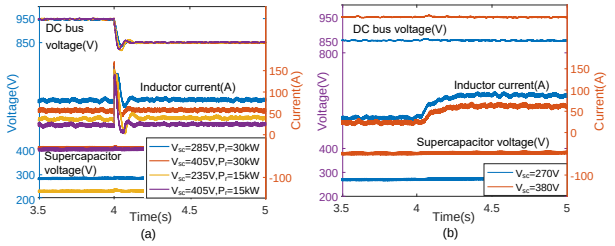

Fig. 19. Voltage step response in charging condition.

The response curves to network voltage reference step in the discharge condition are shown in Figs. 20 (a). The reference voltage steps from 800 V to 815 V. Similar to that in charge condition, the voltage response curves at at different steady-state duty cycles and train powers are almost the same, the settling time is within 100ms, and there is no overshoot. Therefore, the voltage loop has a fast and stable dynamic response process at different steady-state points. A slight difference from charge condition is that the supercapacitor current doesn't return to its initial value when the adjusting process is finished. Instead, it rises about 20A. This is because the output current of the rectifier decreases with the increase of DC bus voltage, and more traction power is supplied by the supercapacitor. And in Fig. 20 (b), the traction power of the motor steps from 10 kW to 25 kW, and the bus voltage has almost no fluctuation, which verifies the system has good ability of anti-disturbance. Therefore, the experimental results of step tests show that under the multi-objective algorithm, the dynamic tracing performance and the anti-disturbance performance of the energy storage system are optimized in the full operating range.

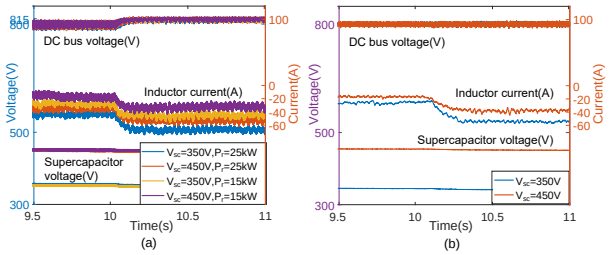

Fig. 20. Voltage responses in discharging condition.

After verifying the dynamic performance of the system, cycling test is conducted to validate the holistic hierarchical control strategy. The scaled train power curve of Beijing Batong Line is input to the motor platform, as seen in Fig. 21, emulating actual operation of the metro train. The experimental result is shown in Fig. 22. In the process of frequent traction and braking of the train, the ESD can accurately jump into the corresponding discharge and charging states, and it exits working in time at 717s and 903s, when the supercapacitor voltage reaches its lower limit, demonstrating the logical rationality and stable operation of the energy management state machine. In addition, it's observed that during the entire cycling test process, the supercapacitor voltage and train power vary in a wide range, especially the train power changes abruptly at the start of train traction and braking, the supercapacitor power follows the change of train power quickly, the control strategy has fast, stable response all the while, keeps good voltage stabilization effect and implements effective braking energy recovery.

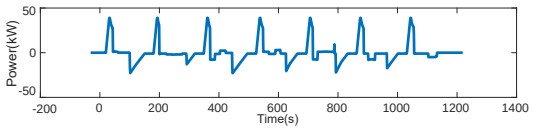

Fig. 21. Input of Driving Cycle for the Motor Platform.

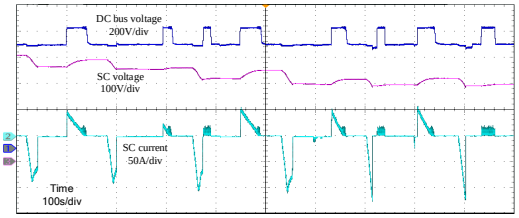

Fig. 22. Experimental Results in Cycling Condition.

B. Field test

The MW-level supercapacitor energy storage system was developed and installed it at Liyuan Station of the Beijing Batong Line, as seen in Fig. 23. The supercapacitor pack has

a total storage energy of 7.4 kWh and peak power of 1.34MW. The energy storage device was put into continuous operation all day for about 2 weeks. In order to analyze the energy saving effect, we recorded the energy statistics of Liyuan substation, as seen in Table III. Before the ESS was put into operation, the average output energy of Liyuan substation was 9392kWh per day, and with ESS working, it saved at least 1016kWh of energy per day, and 1099kWh in average, thus the average output energy of the substation was reduced to 8137kWh. The average energy saving rate reached 12%.

Fig. 23. Photos of the MW level energy storage device.

TABLE III
ENERGY SAVING STATISTICS OF THE MW LEVEL ESD.

	Average day output energy of substation (kWh)	Average day output energy of SC (kWh)
Without ESS	9392	-
With ESS	8137	1099

A specific scenario during field tests at night is presented here to further validate the hierarchical control strategy proposed in this paper. The test section was between Guoyuan Station and Tuqiao Station, as seen in Fig. 24. Two tested trains started accelerating simultaneously, where train 1 departed from Jiukeshu and train 2 left from Linheli, they ran in opposite direction and finally stopped at Liyuan Station. Fig. 25 shows the recorded train running curves. The maximum speed of train 1 was 45km/h, the traction and braking notches were 2 and 3, respectively. And the maximum speed of train 2 was 75km/h.

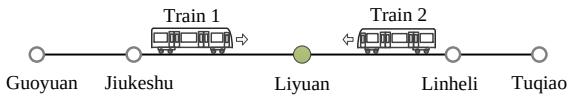

Fig. 24. The test section of Batong Line.

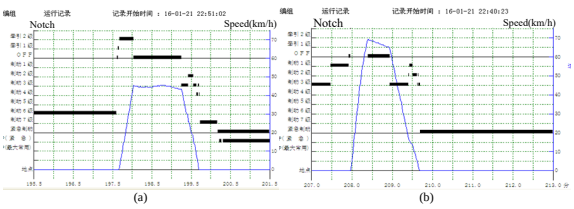

Fig. 25. The running curves of test trains.

Fig. 26 shows the running curve of the ESD. The total supercapacitor current was eight times of the inductor current of a single bridge arm. In the traction and braking processes of the two trains, the supercapacitor current exhibited fast responses, which rose immediately to its maximum value, and the grid voltage fluctuation was suppressed effectively. The dynamic performance of the control strategy was not affected by the variation of train power and supercapacitor voltage. And the energy management state machine correctly recognized the current condition and executed the state transitions instantly. In the simultaneous traction process, the total energy consumption was 24.1 kWh, the supercapacitor voltage decreased from 472 V to 280 V, and it released 2.36 kWh of energy; in the train braking process, the supercapacitor realized fast and effective braking energy recovery effect, the SC voltage increased up to 576 V, 4.15 kWh of energy was recovered by the supercapacitor, accounting for 17.2% of traction consumption.

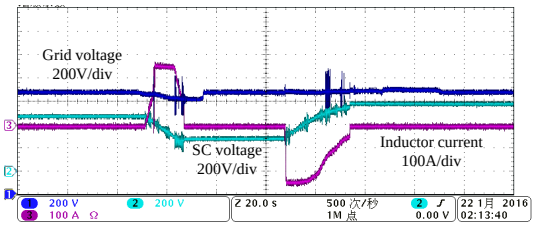

Fig. 26. Operating waveforms of the MW level energy storage device.

VI. CONCLUSION

In this paper, a holistic model, which includes the supercapacitor, DC/DC converter and train is established. By analyzing the model, it is observed that the variation of the train current and duty cycle will have a great influence on the system performance, and the system has a RHPZ in discharge condition. Therefore, based on the double closed-loop control, a multi-objective optimization algorithm is proposed, comprehensively considering the undershoot suppression, rapidity and anti-disturbance performance of the system, and the control parameters are optimized in the full operating range. Both the simulation and laboratory experiment results show that under the proposed control strategy, the system exhibits excellent dynamic performance and strong ability of anti-disturbance in the full operating range. Finally, the field test further verifies the hierarchical strategy, and the results show that the MW-level ESD achieves an energy saving rate of 12%.

REFERENCES

[1] A. Khaligh and Z. Li, "Battery, ultracapacitor, fuel cell, and hybrid energy storage systems for electric, hybrid electric, fuel cell, and plug-in hybrid electric vehicles: State of the art," *IEEE transactions on Vehicular Technology*, vol. 59, no. 6, pp. 2806–2814, 2010.

[2] P. J. Grbovic, P. Delarue, P. Le Moigne, and P. Bartholomeus, "Modeling and control of the ultracapacitor-based regenerative controlled electric drives," *IEEE Transactions on industrial electronics*, vol. 58, no. 8, pp. 3471–3484, 2011.

[3] M. Ogasa, "Application of energy storage technologies for electric railway vehicles-examples with hybrid electric railway vehicles," *IEEJ Transactions on Electrical and Electronic Engineering*, vol. 5, no. 3, pp. 304–311, 2010.

[4] N. Shiraki, K. Tokito, and R. Yokozutsumi, "Propulsion system for catenary and storage battery hybrid electric railcar series ev-e301," in *Electrical Systems for Aircraft, Railway, Ship Propulsion and Road*

Vehicles (ESARS), 2015 International Conference on, pp. 1–7. IEEE, 2015.

[5] T. Ratniyomchai, S. Hillmansen, and P. Tricoli, "Recent developments and applications of energy storage devices in electrified railways," *IET Electrical Systems in Transportation*, vol. 4, no. 1, pp. 9–20, 2013.

[6] F. Devaux and X. Tackoen, "Overview of braking energy recovery technologies in the public transport field," *Energy Recovery Working Paper, www. tickettokyoto. eu*, 2011.

[7] S. Vazquez, S. M. Lukic, E. Galvan, L. G. Franquelo, and J. M. Carrasco, "Energy storage systems for transport and grid applications," *IEEE Transactions on Industrial Electronics*, vol. 57, DOI 10.1109/tie.2010.2076414, no. 12, pp. 3881–3895, 2010.

[8] A. González-Gil, R. Palacin, P. Batty, and J. P. Powell, "A systems approach to reduce urban rail energy consumption," *Energy Conversion and Management*, vol. 80, DOI 10.1016/j.enconman.2014.01.060, pp. 509–524, 2014.

[9] A. González-Gil, R. Palacin, and P. Batty, "Sustainable urban rail systems: Strategies and technologies for optimal management of regenerative braking energy," *Energy conversion and management*, vol. 75, pp. 374–388, 2013.

[10] F. Devaux and X. Tackoen, "Overview of braking energy recovery technologies in the public transport field," *Energy Recovery Working Paper, www. tickettokyoto. eu*, 2011.

[11] V. Musolino, L. Piegari, and E. Tironi, "New full-frequency-range supercapacitor model with easy identification procedure," *IEEE Transactions on Industrial Electronics*, vol. 60, DOI 10.1109/tie.2012.2187412, no. 1, pp. 112–120, 2013.

[12] A.-L. Allegre, A. Bouscayrol, P. Delarue, P. Barrade, E. Chattot, and S. El-Fassi, "Energy storage system with supercapacitor for an innovative subway," *IEEE Transactions on Industrial Electronics*, vol. 57, DOI 10.1109/tie.2010.2044124, no. 12, pp. 4001–4012, 2010.

[13] D. Iannuzzi and P. Tricoli, "Speed-based state-of-charge tracking control for metro trains with onboard supercapacitors," *IEEE Transactions on Power Electronics*, vol. 27, DOI 10.1109/tpel.2011.2167633, no. 4, pp. 2129–2140, 2012.

[14] F. Ciccarelli, D. Iannuzzi, K. Kondo, and L. Fratelli, "Line-voltage control based on wayside energy storage systems for tramway networks," *IEEE Transactions on Power Electronics*, vol. 31, DOI 10.1109/tpel.2015.2411996, no. 1, pp. 884–899, 2016.

[15] P. J. Grbovic, P. Delarue, P. Le Moigne, and P. Bartholomeus, "A bidirectional three-level dc-dc converter for the ultracapacitor applications," *IEEE Transactions on Industrial Electronics*, vol. 57, DOI 10.1109/tie.2009.2038338, no. 10, pp. 3415–3430, 2010.

[16] M. Carpita, M. De Vivo, and S. Gavin, "Dynamic modeling of a bidirectional dc/dc interleaved converter working in discontinuous mode for stationary and traction supercapacitor applications," in *International Symposium on Power Electronics Power Electronics, Electrical Drives, Automation and Motion*, 2012.

[17] R. Barrero, X. Tackoen, and J. V. Mierlo, "Improving energy efficiency in public transport: Stationary supercapacitor based energy storage systems for a metro network," in *2008 IEEE Vehicle Power and Propulsion Conference*, DOI 10.1109/VPPC.2008.4677491, pp. 1–8, Sep. 2008.

[18] D. Iannuzzi, D. Lauria, and F. Ciccarelli, "Wayside ultracapacitors storage design for light transportation systems: a multiobjective optimization approach," *variations*, vol. 6, p. 12, 2013.

[19] F. Ciccarelli, D. Iannuzzi, and P. Tricoli, "Speed-based supercapacitor state of charge tracker for light railway vehicles," in *Power Electronics and Applications (EPE 2011), Proceedings of the 2011-14th European Conference on*, pp. 1–12. IEEE, 2011.

[20] A. Rufer, D. Hotellier, and P. Barrade, "A supercapacitor-based energy storage substation for voltage compensation in weak transportation networks," *IEEE transactions on Power Delivery*, vol. 19, no. 2, pp. 629–636, 2004.

[21] P. J. Grbovic, P. Delarue, P. Le Moigne, and P. Bartholomeus, "The ultracapacitor-based controlled electric drives with braking and ride-through capability: Overview and analysis," *IEEE Transactions on Industrial Electronics*, vol. 58, no. 3, pp. 925–936, 2011.

[22] M. B. Camara, H. Gualous, F. Gustin, and A. Berthon, "Design and new control of dc/dc converters to share energy between supercapacitors and batteries in hybrid vehicles," *IEEE Transactions on Vehicular Technology*, vol. 57, DOI 10.1109/tvt.2008.915491, no. 5, pp. 2721–2735, 2008.

[23] D. Iannuzzi, "Improvement of the energy recovery of traction electrical

[24] M. B. Camara, H. Gualous, F. Gustin, A. Berthon, and B. Dakyo, "Dc/dc converter design for supercapacitor and battery power management in hybrid vehicle applications - polynomial control strategy," *IEEE Transactions on Industrial Electronics*, vol. 57, DOI 10.1109/tie.2009.2025283, no. 2, pp. 587–597, 2010.

[25] W. Lhomme, P. Delarue, P. Barrade, A. Bouscayrol, and A. Rufer, "Design and control of a supercapacitor storage system for traction applications," in *Industry Applications Conference, 2005. Fourtieth IAS Annual Meeting. Conference Record of the 2005*, vol. 3, pp. 2013–2020. IEEE, 2005.

[26] S. I. Serna-Garcés, D. Gonzalez Montoya, and C. A. Ramos-Paja, "Sliding-mode control of a charger/discharger dc/dc converter for dc-bus regulation in renewable power systems," *Energies*, vol. 9, no. 4, p. 245, 2016.

[27] R. Teymourfar, B. Asaei, H. Iman-Eini *et al.*, "Stationary super-capacitor energy storage system to save regenerative braking energy in a metro line," *Energy Conversion and Management*, vol. 56, pp. 206–214, 2012.

[28] S. de la Torre, A. J. Sanchez-Racero, J. A. Aguado, M. Reyes, and O. Martianez, "Optimal sizing of energy storage for regenerative braking in electric railway systems," *IEEE Transactions on Power Systems*, vol. 30, DOI 10.1109/tpwrs.2014.2340911, no. 3, pp. 1492–1500, 2015.

Feiqin Zhu (S'17) received the B.S. degree in electrical engineering from Beijing Jiaotong University, Beijing, China in 2015.

She is currently working towards the Ph.D degree at the School of Electrical Engineering, Beijing Jiaotong University, Beijing, China. Her research interests include modeling and optimization of energy storage systems, cooperative control and energy management in urban railway.

Zhongping Yang (M'14) received the B.Eng. degree from Tokyo University of Mercantile Marine, Tokyo, Japan in 1997, and received the M.Eng. degree and Ph.D. degree from the University of Tokyo, Tokyo, Japan in 1999 and 2002 respectively, all in electrical engineering.

He is currently a Professor with the School of Electrical Engineering, Beijing Jiaotong University, Beijing, China. His research interests include high-speed rail integration technology, traction & regenerative braking technology, and wireless power transfer of urban rail vehicles.

Prof. Yang received the Zhan Tianyou Award for Science and Technology in 2010, the Excellent Popular Science and Technology Book Award in 2011 and the Science and Technology Progress Award (second prize) of Ministry of Education in China in 2016 respectively.

Huan Xia (S'14-M'17) received the B.S. degree from Hefei University of Technology, Hefei, China in 2009, and received the Ph.D. degree in vehicle operation engineering from Beijing Jiaotong University, Beijing, China in 2017.

He is currently working at Beijing Institute of Space Launch Technology, Beijing, China. His research interests include DC/DC converters, energy storage systems and hybrid power systems.

Fei Lin (M'05) received the B.S. degree from Xi'an Jiaotong University, Xi'an, China, the M.S. degree from Shandong University, Jinan, China, and the Ph.D. degree from Tsinghua University, Beijing, China, in 1997, 2000, 2004, respectively, all in electrical engineering.

He is currently a Professor with the School of Electrical Engineering, Beijing Jiaotong University, Beijing, China. His research interests include traction converter and motor drives, energy management for railway systems, digital control of power-electronic-based devices.